Boosting Perovskite Solar Cells Performance and Stability through Doping a Poly-3(hexylthiophene) Hole Transporting Material with Organic Functionalized Carbon Nanostructures

Teresa Gatti, Simone Casaluci, Mirko Prato, Marco Salerno, Francesco Di Stasio, Alberto Ansaldo, Enzo Menna, Aldo Di Carlo,* and Francesco Bonaccorso**

Perovskite solar cells (PSCs) are demonstrating great potential to compete with second generation photovoltaics. Nevertheless, the key issue hindering PSCs full exploitation relies on their stability. Among the strategies devised to overcome this problem, the use of carbon nanostructures (CNSs) as hole transporting materials (HTMs) has given impressive results in terms of solar cells stability to moisture, air oxygen, and heat. Here, the use of a HTM based on a poly(3-hexylthiophene) (P3HT) matrix doped with organic functionalized single walled carbon nanotubes (SWCNTs) and reduced graphene oxide in PSCs is proposed to achieve higher power conversion efficiencies (η = 11% and 7.3%, respectively) and prolonged shelf-life stabilities (480 h) in comparison with a benchmark PSC fabricated with a bare P3HT HTM (η = 4.3% at 480 h). Further endurance test, i.e., up to 3240 h, has shown the failure of all the PSCs based on undoped P3HT, while, on the contrary, a η of ≈8.7% is still detected from devices containing 2 wt% SWCNT-doped P3HT as HTM. The increase in photovoltaic performances and stabilities of the P3HT-CNS-based solar cell, with respect to the standard P3HT-based one, is attributed to the improved interfacial contacts between the doped HTM and the adjacent layers.

1. Introduction

The rise of organo-lead halide perovskite materials as light absorber[1] and metal oxide semiconductor sensitizers[1] in photovoltaic research over dyes[2] and conjugated polymers[3] is testified by the constant increase in power conversion efficiencies (η) obtained by using such materials as active components in perovskite solar cells (PSCs).[4] A certified η of ≈22.1% has been reported in 2016 by Korea Research Institute of Chemical Technology.[5,6] Remarkable features, such as the high absorption coefficient (>10^5 cm^{-1} at 550 nm)[7] and broad absorption spectra over the UV and visible range of the solar spectrum, together with the mobility value of charge carriers (in the range 5–10 cm^2 V^{-1} s^{-1} for electrons and 1–5 cm^2 V^{-1} s^{-1} for holes),[8–11] make them unique candidates to compete with thin-film photovoltaic technologies. Being ionic crystals, organo-lead halide perovskites are not appropriate to be used in conjunction with liquid electrolytes, widely used in standard dye-sensitized solar cells (DSSCs),[2,12] but, on the contrary, must be coupled to a solid state hole conductor.[1] The latter constitutes the hole transporting material (HTM),[1] as in the case of solid-state DSSCs.[1] In PSCs, 2,20,7,70-tetrakis-(*N*,*N*-di-*p*-methoxyphenylamine)9,90-spirobifluorene (Spiro-OMeTAD) is the most widely used HTM. Unfortunately, pristine Spiro-OMeTAD suffers low hole mobility (μ_h) (1.6×10^{-4} cm^2 V^{-1} s^{-1})[13] and electrical conductivity

Dr. T. Gatti, Prof. E. Menna
Department of Chemical Sciences
University of Padova
Padova 35131, Italy
E-mail: enzo.menna@unipd.it
Dr. S. Casaluci, Prof. A. Di Carlo
Department of Electronic Engineering
University of Roma "Tor Vergata"
Center for Hybrid and Organic Solar Energy (CHOSE)
Rome 00173, Italy
E-mail: aldo.dicarlo@uniroma2.it
Dr. M. Prato, Dr. F. Di Stasio
Nanochemistry Department
Istituto Italiano di Tecnologia
Genova 16163, Italy
Dr. M. Salerno
NanoPhysics Department
Istituto Italiano di Tecnologia
Genova 16163, Italy
Dr. A. Ansaldo, Dr. F. Bonaccorso
Graphene Labs
Istituto Italiano di Tecnologia
Genova 16163, Italy
E-mail: francesco.bonaccorso@iit.it

DOI: 10.1002/adfm.201602803

(3×10^{-4} μS cm^{-1})[14] thus requiring a doping process with, e.g., 4-*tert*-butylpyridine (TBP) and bis(trifluoromethane)sulfonimide lithium salt (Li-TFSI), to overcome such limitations.[15] However, these additives are detrimental for the perovskite layer, and consequently also for the stability of the PSC.[16,17] In particular, it has been demonstrated that Spiro-OMeTAD has a poor ability to protect the underlying perovskite[17] from moisture absorption, which is extremely critical in preserving the photovoltaic properties over prolonged time.[16,17] To overcome such issue, the use of conjugated polymers such as poly(3-hexylthiophene) (P3HT) is indeed a reasonable and inexpensive alternative to the Spiro-OMeTAD.[18] In this context, the doping of P3HT with Li-TFSI and TBP has a different effect on the stability of the perovskite layer compared to the Spiro-OMeTAD.[19] In fact, it has been demonstrated that the use of Li-TFSI- and TBP-doped P3HT as HTM reduces the degradation rate of the $CH_3NH_3PbI_3$ layer by a factor of 6 with respect to the Spiro-OMeTAD.[19] The doping of the polymer has been demonstrated to be effective for PSCs stability, with respect to the undoped form,[19] achieving η of 6.7%[20] and 9.3%[18] for the as-prepared devices based on doped-P3HT. Recently, carbon nanostructures (CNSs) such as single-walled carbon nanotubes (SWCNTs) and graphene-based materials (GBMs) have been separately proposed as HTMs.[21–27] Snaith and co-workers have used P3HT-functionalized SWCNTs to improve the thermal stability of PSCs.[21] In fact, by exploiting P3HT-SWCNTs-based HTM they demonstrated an average η of 10 ± 2%, over 96 h exposures at a temperature of ≈80 °C in air. Literature data indicates that CNSs have a double function toward the improvement of both η and stabilities of PSC devices.[21] In fact, from one hand, CNSs "protect" the underlying perovskite layer from atmospheric moisture adsorption and thermal degradation,[21,25] while from the other hand they enable an efficient hole extraction from the perovskite layer,[22,26] if compared with standard HTMs such as Spiro-OMeTAD.

In this framework, the doping of a polymeric HTM such as P3HT with CNSs appears to be a reasonable alternative to the use of pure CNSs, which have often the disadvantage of being difficult to process through solution-based techniques without the use of surfactants,[28,29] especially when high concentration of CNSs (e.g., >10 mg mL^{-1}) is required.[30] These additives are generally used to improve CNS dispersion in liquid media.[28] However, a critical drawback of their use relies on the need of a post-processing approach for their removal afterward.[30] Thus, due to the insulating nature of the surfactants, their removal is required when the electrical conductivity of the deposited CNSs is important and it has to be preserved, as in the case of application as HTMs.[21–27]

A possible solution to the use of surfactants and the subsequent removal process relies on the chemical functionalization of CNSs to facilitate their dispersion in the polymer matrix.[31,32] Owing to the rising importance of functionalized CNS in the framework of PSC technology,[31,32] we investigated the PSC performances, i.e., η and stability, of P3HT HTMs doped with both organic functionalized SWCNTs and reduced graphene oxide (RGO), covalently decorated with *p*-methoxyphenyl substituents. The resulting HTMs are thus composite functional materials,[33] where the optoelectronic properties of the P3HT, such as light absorption/emission and charge transport, are modulated by the presence of small amounts (i.e., ≤5%) of CNSs. Organic chemical modification of the CNSs enabled their homogeneous and stable dispersion within the polymer matrix.[33–35] This improves the contact surface between the polymer and the CNSs and possibly establishes selective intermolecular interactions between them, thus limiting the risk of generating electrical shortcuts within the HTM.[36] The optimal dispersion of CNSs in the polymeric matrix is in fact a requisite to create selective and well-separated pathways for charge percolation in a specific direction (i.e., toward the collecting electrode) at the nanoscale level. This hinders undesirable back-charge transfer processes, particularly for the case of SWCNTs.[37,38] The prevention of aggregation for GBMs is also a key issue to preserve most of their unique properties, such as the high aspect ratio and electrical conductivity, associated to single or few layers graphene sheets.[30,39,40] Furthermore, through functionalization, the maximum concentration of CNSs within a polymer matrix, before the aggregation of the CNSs starts, can be increased with respect to that achievable by using pristine CNSs.[41,42]

In the present study, by the 4 wt% addition of functionalized RGO to the P3HT HTM, we have achieved a η of 9%, maintained over 310 h in air with sealed PSCs. For the case of functionalized SWCNTs a 2 wt% addition has led to a progressive increase in η (i.e., from 6% to 11%) in a 480 h timeframe. Noteworthy, in both configurations, i.e., RGO- and SWCNTs-doped P3HT HTMs, the PSCs have always shown performances superior, both in η and stability, with respect to the one achieved with P3HT HTM.

Our experimental results indicate that neither high μ_h and electrical conductivities nor energy levels alignment are the key factors in enhancing the η of CNSs-based PSCs, in contrast to what was recently proposed.[32] In fact, the increase in η of such devices could be linked with the improvement of local contacts at hybrid interfaces, i.e., the perovskite-HTM and the HTM-top electrode interfaces, determining a more efficient extraction of the photogenerated charge carriers from the polymeric HTM in the presence of CNSs, which also prevents environmental degradation of the perovskite layer.

2. Results and Discussion

Pristine CNSs exhibit a strong tendency to self-aggregation because of the van der Waals interactions between π-conjugated electron clouds,[43] which compromise, for example, the CNSs dispersion within polymeric matrices. An alternative to the use of surfactants,[28,43] which, although ease the dispersion suffer from several aforementioned drawbacks, relies on the functionalization of pristine CNSs with organic groups.[44,45] This enables the CNSs dispersion.[44,45] Here, we chose *p*-methoxyphenyl substituents as organic moieties for the decoration of both SWCNTs and RGO (see **Figure 1**) with the as-prepared functionalized species named SWCNT-PhOMe and RGO-PhOMe, respectively. This type of functionalization is chosen due to its versatility and the possibility to produce CNS derivatives with higher dispersibility in organic media with respect to the pristine ones, as previously demonstrated with multi walled carbon nanotubes (MWCNTs).[46] Based on the reaction introduced by

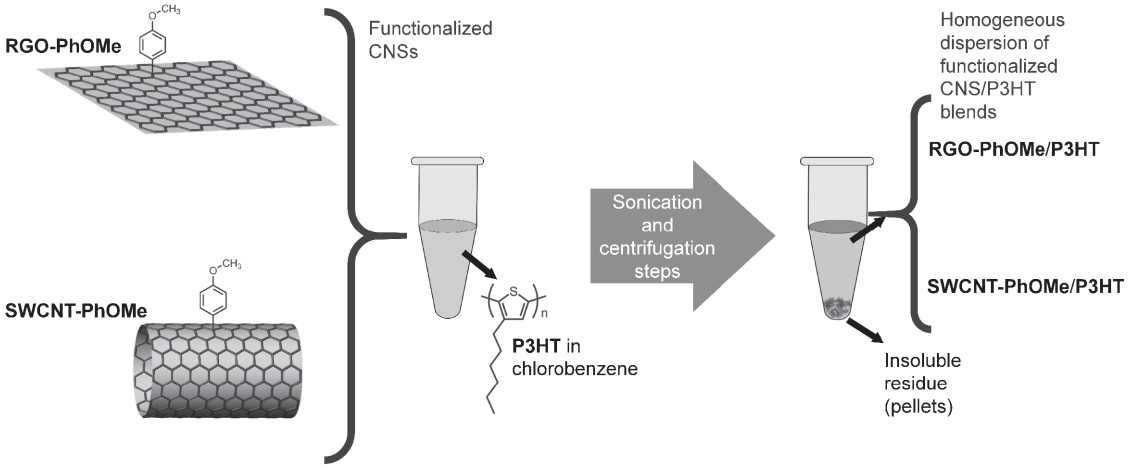

Figure 1. Schematic representation of the sedimentation-based separation process used for the preparation of the *p*-methoxyphenyl functionalized CNS/P3HT blends (see Experimental Section for details).

Tour and Bahr,[47] our functionalization proceeds through the in situ generation of the diazonium salt of *p*-methoxyaniline in the presence of isopentylnitrite, using 1-cyclohexyl-2-pyrrolidone (CHP) as the solvent (see Scheme S1 in the Supporting Information). The amount of reactants together with the reaction times have been tuned to avoid a heavy functionalization of the CNS derivatives, i.e., not completely disrupting their electronic structures.[46] In fact, UV–visible–NIR absorption spectra of the reaction products in dimethylformamide (DMF) (a solvent possessing physico-chemical parameters needed for the CNS dispersions[30,48]) still show, for the case of SWCNT-PhOMe, weak absorption peaks corresponding to the first excitonic transition of metallic SWNTs (M_{11}), and the third excitonic transition of s-SWNTs (eh_{33}), respectively.[49,50] The presence of the absorption features indicates that the electronic structure of the pristine SWCNTs is not completely disrupted (see **Figure 2**a and the inset for details in comparison with Figure S7 in the Supporting Information: reporting the spectra of pristine CNSs). A functionalization degree (FD, defined as the fraction of CNS carbon atoms that are functionalized with respect to the total carbon atoms[51]) of 5% for SWCNT-PhOMe and 3.4% for RGO-PhOMe has been estimated from thermogravimetric analysis as expected (i.e., see refs. [46] and [52]). The calculations are reported in the Supporting Information, together with the corresponding thermograms in Figures S5 and S6 (Supporting Information).

To incorporate SWCNT-PhOMe and RGO-PhOMe within the P3HT matrix, an experimental protocol, based on ultrasonication followed by centrifugation steps, has been carried out (see Experimental Section for details). The centrifugation steps, based on sedimentation-based separation,[53,54] allowed us to remove the insoluble residues (pellets), leaving homogeneous blends of functionalized CNSs and P3HT in chlorobenzene (see Figure 1). The latter is the most appropriate solvent for the deposition of P3HT-based HTMs on top of a perovskite layer.[18]

The percentage in weight of *p*-methoxyphenyl functionalized CNSs with respect to the P3HT is determined by weighting the pellets after the removal of the supernatant, resulting to be 3 and 4 wt% for the SWCNT- and RGO-PhOMe/P3HT blend, respectively. Noteworthy, although the same amounts of *p*-methoxyphenyl functionalized CNSs is used for the preparation of both blends, after the sedimentation-based separation, a higher percentage of carbon nanofillers is found in the polymeric dispersion for the case of RGO-PhOMe with respect to SWCNT-PhOMe. This result could be linked with a higher affinity of the RGO-PhOMe to the polymer matrix with respect to the case of SWCNT-PhOMe. Each dispersion, prepared following the aforementioned procedure, was further diluted with the P3HT solution in chlorobenzene.

This procedure allows us to obtain three different blends having decreasing, with respect to the P3HT, weight percentages of CNSs (namely 1, 2, and 3 wt% for the SWCNT-PhOMe/P3HT blends and 1, 2, and 4 wt% for the RGO-PhOMe/P3HT blends).

UV–visible–NIR absorption spectra of spin-coated thin films of the most concentrated *p*-methoxyphenyl functionalized CNS/P3HT blends (namely 3 wt% SWCNT-PhOMe/P3HT and 4 wt% RGO-PhOMe/P3HT) are recorded and compared with that of a pristine P3HT film. The three spectra (i.e., pristine P3HT, 3 wt% SWCNT-PhOMe/P3HT and 4 wt% RGO-PhOMe/P3HT) are reported in Figure 2b. All the spectra show the intense absorption band of P3HT, characterized by the three vibronic features at 526, 555, and 605 nm, respectively, originated by a combination of π–π^* transitions and lattice vibrations in P3HT crystalline domains.[55–58] In particular, the 0–0 transition (526 nm) is associated to the formation of interchain electronic states, and the 0–1 and 0–2 transitions (555 and 605 nm, respectively) are associated to intrachain excitons within the polymer.[58] The relative intensity of the aforementioned transitions changes from spectrum to spectrum (see Figure 2b). Particularly, we observe an intensity enhancement of absorption feature associated to the 0–0 transition, and a decrease of the one linked to the 0–2 transition for the functionalized CNS/P3HT blends in comparison to the bare P3HT. The change in relative intensity of the vibronic features,[55–58] which is more evident for the case of the 4 wt% RGO-PhOMe/P3HT blend, has been previously reported in the photoluminescence (PL) of P3HT/RGO composites.[59] It has been correlated to an optimized dispersion of the RGO

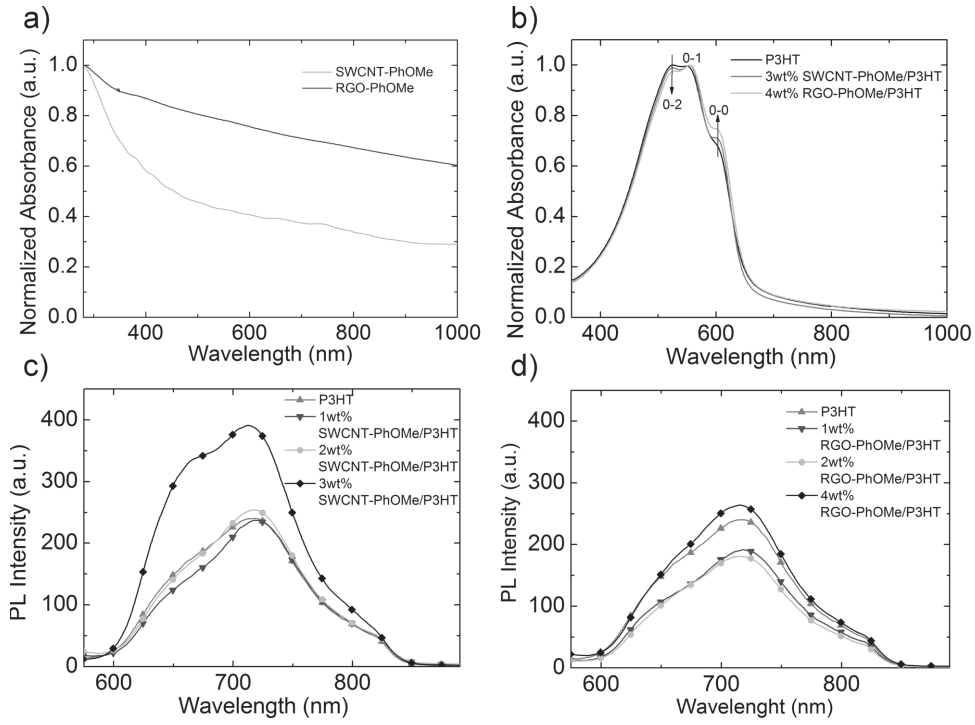

Figure 2. a) Normalized UV–visible–NIR absorption spectra of *p*-methoxyphenyl functionalized CNSs in DMF dispersion. b) Normalized UV–vis–NIR absorption spectra of pristine P3HT, 3 wt% SWCNT-PhOMe/P3HT, and 4 wt% RGO-PhOMe/P3HT blends spin-coated films on glass slides. c) PL spectra of P3HT and SWCNT-PhOMe/P3HT blends and d) of P3HT and RGO-PhOMe/P3HT blends spin-coated films on glass slides (PL intensities were corrected with respect to the absorbance of each film at the excitation wavelength, λ_{exc} = 526 nm).

flakes within the polymer matrix, leading to a weakening of the polymer interchain interactions and to the formation of large hetero-interfaces between the polymer and the RGO flakes themselves.[59] The spectra of the two doped P3HT films do not show absorption features associated to the CNSs (which might be mainly expected in the Vis–NIR range for the SWCNTs[60]), indicating that the reported functionalization process does not affect the HTM light absorption properties.

The optical properties of the *p*-methoxyphenyl functionalized CNS/P3HT blends are further investigated through PL spectroscopy. Photoluminescence spectra of spin-coated films for the six polymer composites and for the reference polymer are shown in Figure 2c,d. The excitation wavelength is set at 526 nm, corresponding to the maximum absorbance of the bare P3HT film (Figure 2b), for all samples even though absorption maxima (λ_{max}) are located at different wavelengths, especially for the RGO-PhOMe/P3HT films (see Figure S8 and Table S1 in the Supporting Information). From the spectra reported in Figure 2c,d, it is evident that no significant quenching of the P3HT solid-state emission is occurring within the films. On the contrary, an increase in P3HT PL is observed with the higher loadings of *p*-methoxyphenyl functionalized CNSs (namely 3 wt% SWCNT-PhOMe and 4 wt% RGO-PhOMe). This behavior has been observed previously in MWCNT and graphene/P3HT composites,[61,62] being correlated to exciton energy transfers[63,64] from the CNSs to the polymer.[59,61,62] The PL phenomena observed for our films appear to be due to interactions between the CNSs and the polymer at different structural level, namely between single P3HT chains and CNSs or between polymeric crystalline nano- or micro-domains[61,62] and well-dispersed or aggregated CNSs. In fact, also the morphology of the composite film might play a role for the PL emission mechanism,[65] together with energy/electron transfer processes taking place within the blends. However, the blue shifts in the emission bands are lower than 4 nm for both the SWCNT-PhOMe/P3HT and RGO-PhOMe/P3HT blends with respect to pristine P3HT. On the contrary, a larger shift of the PL emission bands should otherwise be present when polymer chains experience a significant distortion from planarity due to the presence of the nanofillers.[66] Our PL results thus suggest that the CNSs addition does not significantly affect the intrachain conformation of the polymer.

The functionalized CNS/P3HT polymer composites are then tested as HTMs in PSCs based on $CH_3NH_3PbI_3$, fabricated in air using the double sequential step procedure previously reported.[67] The HTMs are deposited on top of the $CH_3NH_3PbI_3$ perovskite layer by spin-coating, and the PSCs are then finally assembled by evaporating an Au top-electrode atop the polymer films. Seven solar cells with three different configurations are thus obtained, namely one with plain P3HT, three with SWCNT-PhOMe/P3HT and three with RGO-PhOMe/P3HT as HTMs, respectively. Scanning electron microscopy (SEM) images on cross-sections of the PSCs allow us to evaluate the thickness of the different layers within the cells providing an overview of device architectures. As a general example, in **Figure 3** the cross-sectional image of a PSC containing the

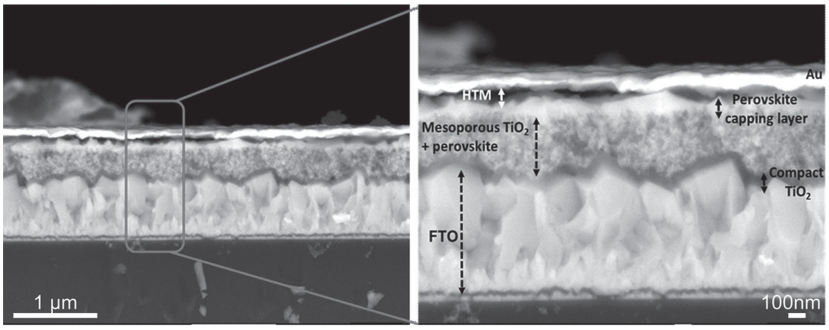

Figure 3. Cross-sectional SEM images of a PSC with 1 wt% RGO-PhOMe/P3HT blend HTM.

1 wt% RGO-PhOMe/P3HT blend as HTM is reported at two different magnifications.

In sequence, from bottom to top in Figure 3 it is possible to identify the presence of the compact TiO_2 layer, having thickness of ≈100 nm, on top of a glass substrate coated with a ≈700 nm thick conducting layer of fluorine doped tin oxide (FTO). Over these layers, there is a mesoporous TiO_2 layer (≈300 nm thick) containing permeated perovskite crystals and an upper perovskite-based capping layer (≈100 nm thick), respectively. Finally, the HTM is above the capping layer, with a thickness of ≈100 nm,[68] on top of which there is the Au layer, acting as back electrode.

The current density-voltage characteristics (*J*–*V* curves) of the as-prepared seven PSCs, measured under simulated AM 1.5 conditions, are extracted at different times before and after device sealing (see Experimental Section for details); devices were stored in dark in the time lapse between each measurement. Amongst the as-prepared devices, the best photovoltaic performance is obtained with 4 wt% RGO-PhOMe/P3HT blend as HTM, with a η of 10%, a fill factor (FF) of 62%, a short-circuit current density (J_{SC}) of 18.8 mA cm^{-2} and an open-circuit voltage (V_{OC}) of 868 mV (see Figure S9 in the Supporting Information for the corresponding *J*–*V* curve). **Figure 4** reports the variation in η and J_{SC} over 480 h of endurance test for the seven PSCs, being each point on the graph the average η value of four devices per each PSC configuration. The endurance test was carried out with the ISOS-D-1 protocol (shelf-life).[69] The curves for the endurance test of FF, and V_{OC} are reported in Figure S10 in the Supporting Information. Statistical data on η for the endurance time of the seven different PSCs are also reported in the Supporting Information (Figure S11) for the sake of completeness.

After the 480 h endurance test, the best device (i.e., in term of photovoltaic performance) is the 2 wt% SWCNT-PhOMe/P3HT-based one, with a η of 11.6% (FF = 62%, J_{SC} = 22 mA cm^{-2}, V_{OC} = 854 mV) (see Figure S9 in the Supporting Information for the corresponding *J*–*V* curve). PSCs fabricated with plain P3HT as the HTM have shown photovoltaic performances lower than cells based on CNS-doped P3HT (η = 6.5% at t = 0 h and η = 5.2% at t = 480 h). From Figure 4a, a steady increase in η is

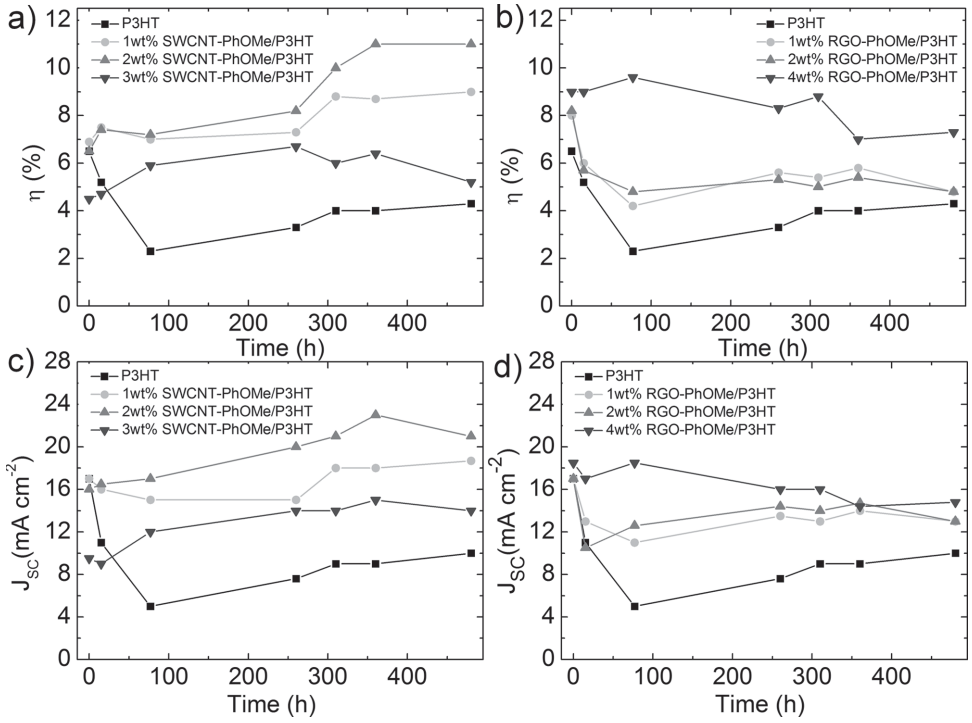

Figure 4. Endurance tests for a) devices based on SWCNT-PhOMe/P3HT blends and b) RGO-PhOMe/P3HT blends used as HTMs. In both graphs the trend in η of the same device based on pristine P3HT HTM is also reported for comparison. c) Variations in J_{SC} as a function of endurance time for devices based on SWCNT-PhOMe/P3HT blends and b) RGO-PhOMe/P3HT blends used as HTMs. In both graphs the trend in J_{SC} of the same device based on pristine P3HT HTM is also reported for comparison. After 15 h, all PSCs were encapsulated.

evident for PSCs based on 1 and 2 wt% SWCNT-PhOMe/P3HT blends, whereas for those based on P3HT a decrease in η from 6.5% to 2.3% is observed in the first 62 h, followed by a slight increase, i.e., up to η = 4.3%, until 480 h of test. The rise in photovoltaic performance for the SWCNT-PhOMe/P3HT-based PSCs is associated to the increase of J_{SC} (Figure 4c). In fact, the other figures of merit, i.e., V_{OC} (≈864 mV) and FF (≈52%), maintain for the entire endurance test the same values as the ones at t = 0 h (see Figure S10 in the Supporting Information).

The increase in η and J_{SC} over time could be correlated to rearrangements at the nano/microscale level within the SWCNT-PhOMe/P3HT composite layer. A possible explanation could be either linked with the formation of additional percolation pathways during PSC activity for electrical charges in the blend itself or with the enhancement of interfacial contacts with the underlying perovskite layer and/or the Au top electrode. Amongst the three tested SWCNT-PhOMe/P3HT blends, the one with the highest percentage of CNSs (i.e., 3 wt%) has not given the best results, neither in the as-prepared devices, in which it has shown even lower performances ($\eta_{average}$ = 4.5%) than the benchmark HTM based on plain P3HT ($\eta_{average}$ = 6.5%), nor after the endurance test. In fact, the 2 wt% SWCNT-PhOMe/P3HT blend reached the highest average η value after 480 h (η ≈ 11%), followed by the 1 wt% blend, i.e., η ≈ 9%. These results may suggest that an optimal SWCNT content within the semiconducting polymer would promote the formation of efficient charge percolation pathways, avoiding electrical short-cuts. Literature data support this explanation.[36]

Concerning RGO-PhOMe/P3HT blends, different behaviors, with respect to the SWCNTs-based ones, were instead observed. In fact, although all the as-prepared devices based on RGO/polymer composites have reported higher average η values (around 8%–9%) with respect to those based on pure P3HT (η = 6.5%), only the 4 wt% RGO-PhOMe/P3HT based PSC has shown stability over the first 310 h of the endurance test, with η ≈9%, showing a decrease to ≈7% in the 310–480 h timeframe. On the contrary, the PSCs with 1 and 2 wt% RGO-PhOMe/P3HT-based HTMs have already shown a significant decrease in η just after encapsulation (15 h), i.e., following the same trend as the P3HT-based reference PSC. However, contrary to the P3HT-based reference PSC, the RGO-PhOMe/P3HT-based devices maintained a stable η values between 4% and 5% for the entire endurance test. Overall, the endurance tests have demonstrated that by using 2 wt% SWCNT-PhOMe/P3HT and 4 wt% RGO-PhOMe/P3HT blends as HTMs in PSCs, after 480 h it is possible to obtain average η values of 11% and 7.3%, respectively. The obtained η values are both significantly higher than that achieved with un-doped P3HT HTM-based PSC (i.e., η = 4.3%).

To further prove the stability of the devices based on functionalized CNS/P3HT HTMs with respect to those containing only pristine P3HT as HTM, we extended the endurance test by keeping the PSCs in dark conditions for 3240 h of aging (Figure S12 in the Supporting Information reports the pictures of the seven PSCs after this endurance test). Even from a simple visual inspection, it is evident that the PSCs fabricated using the bare P3HT HTM have undergone a significant color change from dark brown (the typical color of the as-prepared devices, due to the presence of the pristine perovskite absorber) to yellowish. This color change indicates the formation of PbI_2 as a decomposition product of $CH_3NH_3PbI_3$ after water adsorption.[19] This result could be ascribed to the fact that the bare P3HT film used in this work does not contain any dopant (such as, for example, LiTFSI/TBP). In fact, these dopants absorb the moisture slowing down the decomposition of the underlying $CH_3NH_3PbI_3$ layer in PSCs based on P3HT HTMs.[19] The color change was, however, less evident for PSCs containing functionalized CNS/P3HT HTMs. Photovoltaic measurements confirmed the initial visual inspection. In fact, only the CNS-based PSCs have demonstrated photovoltaic activity after 3240 h of endurance test,[69] as reported in **Table 1**. The obtained results, in term of η for the 3240 h endurance test, are rather different with respect to the ones reported for the first endurance test, i.e., carried out over 480 h of PSCs activity. In fact, amongst devices based on functionalized RGO/P3HT HTM the best average η is shown by the 1 wt% RGO-PhOMe/P3HT-based PSCs, although variations amongst the PSCs with the three different CNS loadings are not significant (differences are lower than 1%). When SWCNT-PhOMe dopants are considered, 2 wt% SWCNT-PhOMe/P3HT-based PSCs still have shown the highest average η (≈8.7%). This is a remarkable result, considering that PSCs based on pristine P3HT as HTMs have shown η = 0. The obtained photovoltaic performances make CNS/P3HT blends very promising HTMs in PSCs.

Table 1. Average η and percentage of active cells for PSCs with HTM based on P3HT and *p*-methoxyphenyl functionalized CNS/P3HT blends after 3240 h of aging in dark.

HTM	After 3240 h	
	Average η [%]	Active cells [%]
P3HT	Null	Null
1 wt% SWCNT-PhOMe/P3HT	5.7	100
2 wt% SWCNT-PhOMe/P3HT	8.7	100
3 wt% SWCNT-PhOMe/P3HT	3.6	100
1 wt% RGO-PhOMe/P3HT	4.7	50
2 wt% RGO-PhOMe/P3HT	3.9	100
4 wt% RGO-PhOMe/P3HT	3.4	75

In order to rationalize the obtained results, we investigated the μ_h role in our composite films, as well as in the plain P3HT. To achieve this goal, space charge limit current (SCLC) experiments[70] are carried out on ad-hoc fabricated diodes (see Experimental Section for details and Figure S13 in the Supporting Information for the corresponding current–voltage, *I–V*, characteristics). **Figure 5**a illustrates the measured μ_h for the functionalized CNS/P3HT blends and for the reference, i.e., the bare P3HT. A reduction in μ_h occurs when the semiconducting polymer is doped with the *p*-methoxyphenyl functionalized CNSs. These results indicate that the increase in η of the CNS/P3HT-based PSCs is not linked with the μ_h enhancement in the HTM with respect to the bare P3HT. In particular, the lowest value of $\mu_h = 0.27 \times 10^{-4}$ cm^2 V^{-1} s^{-1} is recorded for the case of the 2 wt% RGO-PhOMe/P3HT blend. Higher values, close to the ones measured for P3HT, are

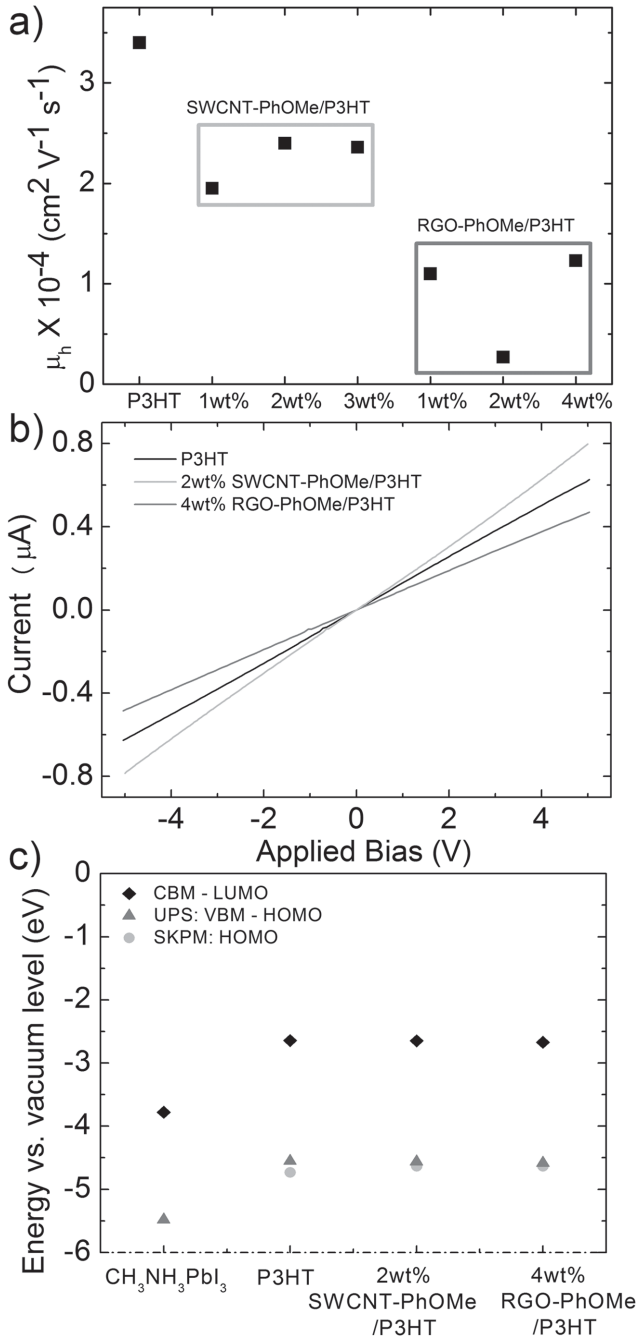

Figure 5. a) μ_h in P3HT and *p*-methoxyphenyl functionalized CNS/P3HT blends calculated by means of the SCLC method. b) *I–V* curves for a P3HT film and for the two best performing *p*-methoxyphenyl functionalized CNS/P3HT blends used as HTMs. The measurements are carried out on Au interdigitated electrode arrays with a 3 μm gap/spacing between electrodes. c) Energy position of the VBM and CBM of the $CH_3NH_3PbI_3$ layer compared with those of the HOMO and LUMO for pristine P3HT and for best performing *p*-methoxyphenyl functionalized CNS/P3HT blends as HTMs. VBM and HOMO level positions have been obtained through UPS and SKPM experiments. For each considered sample, CBM or LUMO levels have been obtained by adding the optical bandgaps (derived from absorption spectra) to the VBM or HOMO level positions, as obtained by UPS.

achieved by the SWCNT-PhOMe/P3HT blends. In particular, a $\mu_h = 2.4 \times 10^{-4}$ cm^2 V^{-1} s^{-1} has been achieved with 2 wt% loading. However, the mobility is only one of the parameters contributing to the electrical conductivity in a material, together with the number of charge carriers and the electric charge. Indeed, the 2 wt% SWCNT-PhOMe/P3HT blend, which is the one ensuring the best PSC performance when used as HTM, is significant in this aspect. In fact, *I–V* measurements carried out on Au interdigitated electrodes arrays for spin-coated films of the different blends show a higher current (0.797 μA at 5 V) for 2 wt% SWCNT-PhOMe/P3HT (Figure 5b) with respect to pristine P3HT (0.626 μA at 5 V). This translates in an electrical conductivity of 19.9 and 11.6 μS cm^{-1} for the two films, respectively. On the contrary, the 4 wt% RGO-PhOMe/P3HT film (which is the best HTM amongst those based on P3HT doped with functionalized RGO) shows a lower current (0.470 μA at 5 V, 15.3 μS cm^{-1}) compared to the other two films. The energy band alignment between the Au electrode (work function around 4.6 eV[71]) and the P3HT HOMO/LUMO suggests that the measured current is mostly driven by hole transport, due to the presence of a large energy barrier for electron injection (around 1.95 eV for all samples). It is worthy to emphasize that the electrical characterization results of our *p*-methoxyphenyl functionalized CNS/P3HT blends are significantly different from the ones reported by Ye et al.[32] In fact, by exploiting a P3HT film doped with a GBM functionalized with an imidazole moiety, they found both higher μ_h and electrical conductivity with respect to the ones based on pristine P3HT films.[32] This is in contrast with our data. The differences may rely both on the different type of GBMs used in the two works as well as on the functionalization process and the different preparation approaches for the blending with the P3HT. The zoo existing in the GBMs nomenclature is not helping in this perspective.[72] Further investigations are carried out in order to figure out possible explanations for the increased η and for the remarkable stabilities over prolonged times measured in PSC devices containing 2 wt% SWCNT-PhOMe/P3HT and 4 wt% RGO-PhOMe/P3HT blends as HTMs in comparison to those containing only bare P3HT. It is well-known[73,74] that the η in photovoltaic devices based on heterojunctions is strictly linked to the ability to extract the photogenerated charge carriers from the photoactive material and carry them to the top and bottom electrodes, i.e., to the band alignment between the active layer and the hole and electron transporting materials.[73,74] We therefore investigated, through ultraviolet photoelectron spectroscopy (UPS) and scanning Kelvin probe microscopy (SKPM), the alignment between the valence band of the perovskite layer and the HOMO levels of the HTMs. We examined the case of the best performing HTMs in terms of η and stability, i.e., the 2 wt% SWCNT-PhOMe/P3HT and 4 wt% RGO-PhOMe/P3HT blends in comparison with bare P3HT. The obtained energy level values are shown in Figure 5c (experimental data are reported in Figures S14 and S16 and Tables S2 and S3 in the Supporting Information).

The position of the valence band maximum (VBM) of the $CH_3NH_3PbI_3$ layer, obtained by UPS analysis, is at –5.48 eV versus vacuum level, in agreement with values previously reported in literature.[75,76] By adding the energy bandgap of

the material (i.e., 1.7 eV, as reported in ref. [75]) to the VBM position, the energy position of the conduction band minimum (CBM), is estimated to be −3.78 eV versus vacuum. This CBM value would allow an efficient transfer of photogenerated electrons from the $CH_3NH_3PbI_3$ layer to the electron transporting material, i.e., TiO_2, which has a CBM position of ≈−4.3 eV versus vacuum.[77] Concerning the HTMs designed in this work, the HOMO levels obtained via UPS (and confirmed by SKPM) do not show a significant dependency on the presence of CNSs. In fact, values of −4.56 and −4.58 eV versus vacuum were calculated for the 2 wt% SWCNT-PhOMe/P3HT and 4 wt% RGO-PhOMe/P3HT blends respectively, which are quite close to the one of the pristine P3HT, i.e., −4.55 eV versus vacuum. These values are in agreement with recent data reported for P3HT.[78] In order to estimate the LUMO levels, we calculated the energy band gaps of both the pristine P3HT and the two blends from the absorption spectra (see Figure S15 in the Supporting Information), obtaining a value of 1.91 ± 0.05 eV for all the samples. The LUMO levels are therefore at ≈−2.65 eV versus vacuum, as shown in Figure 5c. Although the bands alignment favors the hole transport from the perovskite to the HTM layer, inhibiting, at the same time, the electron transfer, it however does not explain the increased η values and stabilities observed for the 2 wt% SWCNT-PhOMe/P3HT- and 4 wt% RGO-PhOMe/P3HT-based PSCs with respect to the one based on pristine P3HT. From our data, it appears, indeed, that no significant thermodynamic driving force is causing such improvements. This is in contrast with what found previously by Ye and coworkers,[32] which reported lower HOMO energies for functionalized RGO-doped P3HT via UPS, facilitating hole transfer from $CH_3NH_3PbI_3$ and thus driving the η enhancement.

Our experimental evidences suggest that the improved η performances and stabilities of the PSCs containing CNS-doped P3HT HTMs with respect to one based on P3HT is due to manifold effects. First, the engineering of hybrid interfaces,[79,80] with the improvement of local electrical contacts at the nanoscale due to the CNSs addition, between the $CH_3NH_3PbI_3$ absorber and the HTM and/or between the HTM and the top Au electrode. This could be responsible for a more efficient transport of photogenerated charges across the interfaces. Moreover, the CNSs addition might improve the depletion of holes from the perovskite layer, thus limiting charge recombination in the photoactive layer.[22,26] Finally, the presence of CNSs avoids degradation of the perovskite layer induced by environmental factors such as moisture or oxygen, which is particularly important for the devices stability. In fact, the CNSs provide a more hydrophobic protective layer with respect to the use of pristine polymers.[21–26]

3. Conclusions

We present a photovoltaic characterization of PSCs based on novel HTMs, originated by doping P3HT with organic functionalized CNSs. The process of mixing the semiconducting polymer with the conducting carbon-based nanofillers is carried out, by first selecting CNS derivatives with good dispersibility in organic media and then combining them with the matrix in solution. We exploit a sedimentation-based separation process to remove both the aggregates and bundles from the HTM in liquid phase, i.e., before deposition. The designed HTMs are tested in three different concentrations of CNSs per type, i.e., SWCNTs and RGO, in PSCs, showing a significant improvement of photovoltaic performances with respect to PSCs based on bare P3HT. The exploitation of CNS-based HTM is beneficial for the PSCs stability. In fact, endurance tests, carried out over 3240 h, have shown $\eta_{average}$ of 8.7% and 4.7% for SWNTs- and RGO-based PSCs, which is a remarkable results if compared with $\eta = 0$ of the devices based on the un-doped polymer. Although further work is needed to fully understand the physico-chemical mechanisms responsible for the increase of the photovoltaic performance upon CNS addition, our results pave the way towards the development of PSCs with prolonged lifetime, thus able to challenge the current photovoltaic market.

4. Experimental Section

Materials: All reagents and solvents were purchased from Sigma-Aldrich and used as received. P3HT was purchased from Merck (M_w = 94.100 g mol^{-1}, PD = 1.9, RR = 95.5%). HiPco SuperPurified SWCNTs were purchased from Unidym (lot # P2150) and used as received. Nanotube diameters are reported by the producer to be between 0.8 and 1.2 nm and lengths between 100 and 1000 nm. Reduced graphene oxide powder was purchased from ACS Material, LLC (product No.: GnP1L-0.5g) and used as received. The production method, as reported by the supplier, consists in completely reducing graphene oxide obtained via the Hummer's method through thermal exfoliation reduction and further hydrogen reduction. Reduced graphene oxide flakes have lateral dimensions between 1 and 2 µm, are constituted of few layers overlapping irregularly and have many corrugations, as evident from transmission electron microscopy (TEM) images (see Figure S1 in the Supporting Information).

Synthesis of SWCNT-PhOMe and RGO-PhOMe: Carbon nanostrutures (20 mg, 1.66 mmol of C, either SWCNTs or RGO) are ultrasonicated in CHP (15 mL) with 3000 (Misonix) tip sonicator using the following pulse parameters: time on = 3 s, time off = 3 s, power level = 2 (4–6 W) for 10 min. The as-obtained dispersions are then transferred in a flask under nitrogen and heated up to 80 °C. 4-methoxyaniline (102 mg, 0.83 mmol) is added while stirring the dispersion, followed by the addition of isopentylnitrite (0.11 mL, 0.83 mmol). The reaction is continued for 4 h, whereupon it is allowed to cool down to room temperature. Methanol (200 mL) is then added and the mixture stirred for 10 min. 4-methoxyphenyl functionalized CNSs are recovered by filtration and washed with methanol (100 mL). CNS filtration is performed using Fluoropore membrane filters (0.2 µm) purchased from Merck Millipore. The filter is then dried under an IR lamp to detach SWCNT-PhOMe and RGO-PhOMe. 1 mg per each of these materials is subjected to thermogravimetric analysis (TGA), to determine the FD.[51]

Characterization of SWCNT-PhOMe and RGO-PhOMe: Starting materials (SWCNTs and RGO) are previously characterized through micro-Raman analysis, and thermogravimetric analysis. Data on Hipco SWCNTs are available from the producer and have also been reported in our previous work (see ref. [52]). Data on RGO powder are reported in the Supporting Information (Figures S2 and S3). For this material, carbon to oxygen ratio has been also estimated through x-ray photoelectron spectroscopy (XPS), resulting to be 90:10 (see Supporting Information and Figure S4 therein for details). Thermogravimetric analysis of CNS samples is carried out with a Q5000IR TGA (TA Instruments) under nitrogen by an isotherm at 100 °C for 10 min followed by heating at 10 °C min^{-1} rate up to 900 °C.

Preparation of SWCNT-PhOMe/P3HT and RGO-PhOMe/P3HT Blend Dispersions: P3HT dispersions in chlorobenzene at the concentration of 15 mg mL^{-1} are prepared by dissolving the solid polymer in the solvent,

followed by stirring overnight at 70 °C on a hot plate. 4-methoxyphenyl functionalized CNSs (15 mg) are added to 10 mL of P3HT dispersion in chlorobenzene and the resulting mixture is ultrasonicated for 10 min and then subjected to centrifugation at 3000 rpm for 3 min. Ultracentrifugation is performed on an MR23i Jouan ultracentrifuge equipped with a SWM 180.5 swinging bucket rotor (Thermo Electron Corporation). The supernatant is separated and the solid residue at the bottom of the centrifuge tube is then washed with chloroform (2 × 20 mL), filtered and dried under IR lamp, in order to allow precise weighting. This procedure is crucial for the determination of the amount of 4-methoxyfunctionalized CNSs left in the P3HT dispersion. Following this protocol, the most concentrated CNS/P3HT blend dispersions are obtained (3 wt% for SWCNT-PhOMe/P3HT and 4 wt% for RGO-PhOMe/P3HT, respectively). Starting from these concentrated dispersions, we then diluted them, i.e., by mixing 1 mL of 3 wt% SWCNT-PhOMe/P3HT with 2 mL of the mother P3HT dispersion in chlorobenzene we obtained the 2 wt% SWCNT-PhOMe/P3HT blend, whereas the 1 wt% SWCNT-PhOMe/P3HT blend is obtained by mixing 2 mL of 3 wt% SWCNT-PhOMe/P3HT with 1 mL of P3HT dispersion. As for RGO-PhOMe/P3HT blends, 2 and 1 mL of the most concentrated 4 wt% RGO-PhOMe/P3HT one are mixed with 2 and 3 mL of P3HT dispersion to produce respectively the 2 wt% RGO-PhOMe/P3HT and the 1 wt% RGO-PhOMe/P3HT blends.

Characterization of SWCNT-PhOMe/P3HT and RGO-PhOMe/P3HT Blend Dispersions: Absorption and photoluminescence spectra are measured with a Varian Cary 5000 spectrophotometer and a Perkin Elmer LS 55 luminescence spectrometer, respectively. Samples are prepared by spin-coating 100 µL of blend dispersion at 2000 rpm for 40 s on Corning cover glass slides N_o 1 1.25 mm × 1.25 mm.

PSCs Fabrication: Transparent glass substrates pre-coated with FTO (Pilkington, 8 Ohm Square^{-1}, 25 mm × 25 mm) are etched by raster scanning laser (Nd:YVO4 pulsed at 30 kHz with average output power of P = 10 W) to define the desired electrode pattern. Patterned substrates were cleaned by ultrasonic bath, using detergent, acetone and isopropanol. A compact TiO_2 film was deposited onto the FTO surface by spray pyrolysis.[81] After that, a thin film of TiO_2 nanoparticles based paste (18NR-T Dyesol diluted with ethanol) is screen-printed and successively sintered at 480 °C for 30 min. In air, double sequential step procedure is used to realize the perovskite active layer.[67] 100 µL of HTM dispersion are deposited by spin-coating at 2000 rpm for 40 s under a nitrogen atmosphere. Samples are then introduced into a high vacuum chamber (10^{-6} mbar) for the thermal evaporation of the Au top electrode (thickness 100 nm) through a shadow mask. Each PSC resulted to have an active area of 0.1 cm^2 for the anode (2 mm) and cathode (5 mm) overlap. Four cells are fabricated on each substrate. After fabrication, PSCs are kept in a glove box and after 15 h are encapsulated with methacrylate glue and glass, and then left in air. Masked devices (3 × 6 mm aperture) are tested under AM-1.5 conditions to extract *J–V* curves. In between each measurement performed to derive the variation in photovoltaic parameters along time, PSCs are kept in dark conditions.

PSCs Characterization: Device cross-sections are prepared by breaking the cells after scribing the glass with a diamond tip. Freshly cut cross-sections of the samples are imaged with a field-emission scanning electron microscope FE-SEM (Jeol JSM-7500 FA) without adding any conductive coating. The acceleration voltage is set at 10 kV, and images are collected by using compositional contrast (backscattered electrodes).

J–V curves of PSC devices are extracted employing a Keythley 2420 source-meter under irradiation at AM-1.5 100 mW cm^{-2} generated using a Class A solar simulator (ABET Technologies, Sun 2000). The light irradiation level is verified at the quote and position where the PSC is placed by means of a calibrated Pyranometer (Skye SKS1110).

Hole Mobility Measurements: To extrapolate the P3HT μ_h values in both bare polymer film and CNS-doped ones, diodes with the structure ITO/PEDOT:PSS/P3HT or CNS-doped P3HT/Al are fabricated. On a clean glass/ITO substrate, having identical pattern as the ones devised for the PSCs, a PEDOT:PSS dispersion in water (Clevios) is spin-coated and annealed at 150 °C for 10 min. On top of this layer, ≈150 nm thick P3HT is spin-coated and finally aluminum top contact is evaporated (100 nm thickness). Dedicated shadow mask is used to realize devices with an active area of 0.05 cm^2. Automatic custom-made equipment is used to extrapolate *J–V* dark curves from −5 to +5 V (see Supporting Information).

Electrical Measurements: The electrical measurements are carried out on Au interdigitated electrodes array on Si/SiO_2 with spacing between the electrodes arms of 3 µm, a thickness of 100 nm and two separated connection tracks. Films of the different CNS-based blends and pristine P3HT are obtained by spin-coating at 2000 rpm for 40 s in glove-box. Measurements are carried out in air, using a Suss Microtec PM5 probe station connected to Keithley 2612 controlled via a Labview interface.

Energy Level Determination: Ultraviolet photoelectron spectroscopy (UPS) analysis is performed on spin-cast films of $CH_3NH_3PbI_3$, pristine P3HT, 2 wt% SWCNT-PhOMe/P3HT and 4 wt% RGO-PhOMe/P3HT blends on FTO slides to estimate the position of the VBM (in the case of the perovskite film) and of the HOMO level (in the case of P3HT and blends) of the materials under investigation. The measurements are carried out with a Kratos Axis Ultra^{DLD} spectrometer using a He I (21.22 eV) discharge lamp. The analyses are conducted on an area of 55 µm in diameter, at pass energy of 10 eV and with a dwell time of 100 ms. The work function (i.e., the position of the Fermi level with respect to vacuum level) is measured from the threshold energy for the emission of secondary electrons during He I excitation. A −9.0 V bias is applied to the sample in order to precisely determine the low kinetic energy cut-off, as discussed in ref. [82]. Then, the position of the VBM/HOMO versus vacuum level is estimated by measuring their distance from the Fermi level, according to the graphical method used in refs. [75] and [76].

Scanning Kelvin probe microscopy (SKPM) mode of atomic force microscopy (AFM) is carried out on a MFP-3D instrument by Asylum Research (Santa Barbara, CA, USA). The probe is a PPP-NCSTPt (Nanosensors, Neuchatel, Switzerland) with a ≈25 nm thick coating of PtIr, and nominal resonance frequency of ≈160 kHz. Its work function is calibrated versus a reference of highly oriented pyrolytic graphite, freshly cleaved, assumed to be 4.65 eV.[83] The height of the second lift pass is 100 nm.

Supporting Information

Supporting Information is available from the Wiley Online Library or from the author.

Acknowledgements

This project received funding from the European Union's Horizon 2020 research and innovation programme under grant agreement no. 696656 – GrapheneCore1 and from PRIN project DSSCX(MIUR).

Received: June 6, 2016
Revised: July 18, 2016
Published online: September 13, 2016

[1] P. Docampo, S. Guldin, T. Leijtens, N. K. Noel, U. Steiner, H. J. Snaith, *Adv. Mater.* **2014**, *26*, 4013.
[2] A. Hagfeldt, G. Boschloo, L. Sun, L. Kloo, H. Pettersson, *Chem. Rev.* **2010**, *110*, 6595.
[3] S.-S. Li, C.-W. Chen, *J. Mater. Chem. A* **2013**, *1*, 10574.
[4] N.-G. Park, *Mater. Today* **2014**, *18*, 65.
[5] W. S. Yang, J. H. Noh, N. J. Jeon, Y. C. Kim, S. Ryu, J. Seo, S. Il Seok, *Science* **2015**, *348*, 1234.
[6] NREL (National Renewable Energy Laboratory) Best Research-Cell Efficiencies, http://www.nrel.gov/ncpv/images/efficiency_chart.j (accessed: May 5, 2016).

[7] M. A. Green, A. Ho-Baillie, H. J. Snaith, *Nat. Photonics* **2014**, *8*, 506.
[8] G. Xing, N. Mathews, S. Sun, S. S. Lim, Y. M. Lam, M. Gratzel, S. Mhaisalkar, T. C. Sum, *Science* **2013**, *342*, 344.
[9] M. A. Loi, J. C. Hummelen, *Nat. Mater.* **2013**, *12*, 1087.
[10] T. C. Sum, N. Mathews, *Energy Environ. Sci.* **2014**, *7*, 2518.
[11] C. Motta, F. El-Mellouhi, S. Sanvito, *Sci. Rep.* **2015**, *5*, 12746.
[12] G. Calogero, A. Bartolotta, G. Di Marco, A. Di Carlo, F. Bonaccorso, *Chem. Soc. Rev.* **2015**, *44*, 3244.
[13] H. J. Snaith, M. Grätzel, *Appl. Phys. Lett.* **2006**, *89*, 262114.
[14] A. Abate, T. Leijtens, S. Pathak, J. Teuscher, R. Avolio, M. E. Errico, J. Kirkpatrik, J. M. Ball, P. Docampo, I. McPherson, H. J. Snaith, *Phys. Chem. Chem. Phys.* **2013**, *15*, 2572.
[15] S. Wang, W. Yuan, Y. S. Meng, *ACS Appl. Mater. Interfaces* **2015**, *7*, 24791.
[16] Y. Rong, L. Liu, A. Mei, X. Li, H. Han, *Adv. Energy Mater.* **2015**, *5*, 1.
[17] D. Wang, M. Wright, N. K. Elumalai, A. Uddin, *Sol. Energy Mater. Sol. Cells* **2016**, *147*, 255.
[18] F. Di Giacomo, S. Razza, F. Matteocci, A. D'Epifanio, S. Licoccia, T. M. Brown, A. Di Carlo, *J. Power Sources* **2014**, *251*, 152.
[19] J. Yang, B. D. Siempelkamp, D. Liu, T. L. Kelly, *ACS Nano* **2015**, *9*, 1955.
[20] J. H. Heo, S. H. Im, J. H. Noh, T. N. Mandal, C.-S. Lim, J. A. Chang, Y. H. Lee, H. Kim, A. Sarkar, N. K. M. Gratzel, S. Il Seok, *Nat. Photonics* **2013**, *7*, 486.
[21] S. N. Habisreutinger, T. Leijtens, G. E. Eperon, S. D. Stranks, R. J. Nicholas, H. J. Snaith, *Nano Lett.* **2014**, *14*, 5561.
[22] S. N. Habisreutinger, T. Leijtens, G. E. Eperon, S. D. Stranks, R. J. Nicholas, H. J. Snaith, *J. Phys. Chem. Lett.* **2014**, *5*, 4207.
[23] Q. Luo, Y. Zhang, C. Liu, J. Li, N. Wang, H. Lin, *J. Mater. Chem. A* **2015**, *3*, 15996.
[24] J. Cao, Y.-M. Liu, X. Jing, J. Yin, J. Li, B. Xu, Y.-Z. Tan, N. Zheng, *J. Am. Chem. Soc.* **2015**, *137*, 10914.
[25] Y. Jiao, F. Ma, G. Gao, H. Wang, J. Bell, T. Frauenheim, A. Du, *RSC Adv.* **2015**, *5*, 82346.
[26] R. Ihly, A.-M. Dowgiallo, M. Yang, P. Schulz, N. J. Stanton, O. G. Reid, A. J. Ferguson, K. Zhu, J. J. Berry, J. L. Blackburn, *Energy Environ. Sci.* **2016**, *9*, 1439.
[27] A. L. Palma, L. Cinà, S. Pescetelli, A. Agresti, M. Raggio, R. Paolesse, F. Bonaccorso, A. Di Carlo, *Nano Energy* **2016**, *22*, 349.
[28] W. Wenseleers, I. I. Vlasov, E. Goovaerts, E. D. Obraztsova, A. S. Lobach, A. Bouwen, *Adv. Funct. Mater.* **2004**, *14*, 1105.
[29] F. Bonaccorso, T. Hasan, P. H. Tan, C. Sciascia, G. Privitera, G. Di Marco, P. G. Gucciardi, A. C. Ferrari, *J. Phys. Chem. C* **2010**, *114*, 17267.
[30] F. Bonaccorso, A. Bartolotta, J. N. Coleman, C. Backes, *Adv. Mater.* **2016**, *28*, 6136.
[31] S. Casaluci, A. Di Carlo, F. Bonaccorso, T. Gatti, E. Menna, *Nanotechnol., 2015 IEEE 15th Int. Conf.* IEEE, Rome, Italy, **2015**, pp. 41–44.
[32] J. Ye, X. Li, J. Zhao, X. Mei, Q. Li, *RSC Adv.* **2016**, *6*, 36356.
[33] T. Gatti, N. Vicentini, M. Mba, E. Menna, *European J. Org. Chem.* **2016**, *2016*, 1071.
[34] Z. Xiang, Q. Dai, J.-F. Chen, L. Dai, *Adv. Mater.* **2016**, *28*, 6253.
[35] P. Bačová, A. N. Rissanou, V. Harmandaris, *Macromolecules* **2015**, *48*, 9024.
[36] S. Cataldo, P. Salice, E. Menna, B. Pignataro, *Energy Environ. Sci.* **2012**, *5*, 5919.
[37] D. Benetti, K. T. Dembele, J. Benavides, H. Zhao, S. Cloutier, I. Concina, A. Vomiero, F. Rosei, *J. Mater. Chem. C* **2016**, *4*, 3555.
[38] J. Lee, M. M. Menamparambath, J.-Y. Hwang, S. Baik, *ChemSusChem* **2015**, *8*, 2358.
[39] A. Capasso, A. E. D. R. Castillo, H. Sun, A. Ansaldo, V. Pellegrini, F. Bonaccorso, *Solid State Commun.* **2015**, *224*, 53.
[40] Y. Hernandez, V. Nicolosi, M. Lotya, F. M. Blighe, Z. Sun, S. De, I. T. McGovern, B. Holland, M. Byrne, Y. K. Gun'Ko, J. J. Boland, P. Niraj, G. Duesberg, S. Krishnamurthy, R. Goodhue, J. Hutchison, V. Scardaci, A. C. Ferrari, J. N. Coleman, *Nat. Nanotechnol.* **2008**, *3*, 563.
[41] N. Vicentini, T. Gatti, P. Salice, G. Scapin, C. Marega, F. Filippini, E. Menna, *Carbon N. Y.* **2015**, *95*, 725.
[42] Y. Lin, M. J. Meziani, Y.-P. Sun, *J. Mater. Chem.* **2007**, *17*, 1143.
[43] F. Bonaccorso, N. Balis, M. M. Stylianakis, M. Savarese, C. Adamo, M. Gemmi, V. Pellegrini, E. Stratakis, E. Kymakis, *Adv. Funct. Mater.* **2015**, *25*, 3870.
[44] D. Tasis, N. Tagmatarchis, A. Bianco, M. Prato, *Chem. Rev.* **2006**, *106*, 1105.
[45] V. Georgakilas, M. Otyepka, A. B. Bourlinos, V. Chandra, N. Kim, K. C. Kemp, P. Hobza, R. Zboril, K. S. Kim, *Chem. Rev.* **2012**, *112*, 6156.
[46] P. Salice, E. Fabris, C. Sartorio, D. Fenaroli, V. Figà, M. P. Casaletto, S. Cataldo, B. Pignataro, E. Menna, *Carbon N. Y.* **2014**, *74*, 73.
[47] J. L. Bahr, J. M. Tour, *Chem. Mater.* **2001**, *13*, 3823.
[48] F. Bonaccorso, A. Lombardo, T. Hasan, Z. Sun, L. Colombo, A. C. Ferrari, *Mater. Today* **2012**, *15*, 564.
[49] R. B. Weisman, S. M. Bachilo, *Nano Lett.* **2003**, *3*, 1235.
[50] H. Kataura, Y. Kumazawa, Y. Maniwa, I. Umezu, S. Suzuki, Y. Ohtsuka, Y. Achiba, *Synth. Met.* **1999**, *103*, 2555.
[51] M. D'Este, M. De Nardi, E. Menna, *Eur. J. Org. Chem.* **2006**, *2006*, 2517.
[52] P. Salice, C. Sartorio, A. Burlini, R. Improta, B. Pignataro, E. Menna, *J. Mater. Chem. C* **2015**, *3*, 303.
[53] F. Bonaccorso, M. Zerbetto, A. C. Ferrari, V. Amendola, *J. Phys. Chem. C* **2013**, *117*, 13217.
[54] P. Salice, A. Gambarin, N. Daldosso, F. Mancin, E. Menna, *J. Phys. Chem. C* **2014**, *118*, 27028.
[55] J. J. Apperloo, R. A. J. Janssen, M. M. Nielsen, K. Bechguard, *Adv. Mater.* **2000**, *12*, 1594.
[56] T. Yamamoto, D. Komarudin, M. Arai, B.-L. Lee, H. Suganuma, N. Asakawa, Y. Inoue, K. Kubota, S. Sasaki, T. Fukuda, H. Matsuda, *J. Am. Chem. Soc.* **1998**, *120*, 2047.
[57] H. Tachibana, N. Hosaka, Y. Tokura, *Macromolecules* **2001**, *34*, 1823.
[58] P. J. Brown, D. S. Thomas, A. Köhler, J. S. Wilson, J.-S. Kim, C. M. Ramsdale, H. Sirringhaus, R. H. Friend, *Phys. Rev. B* **2003**, *67*, 64203.
[59] F. Zheng, W.-L. Xu, H.-D. Jin, X.-T. Hao, K. P. Ghiggino, *RSC Adv.* **2015**, *5*, 89515.
[60] T. Hasan, P. H. Tan, F. Bonaccorso, A. G. Rozhin, V. Scardaci, W. I. Milne, A. C. Ferrari, *J. Phys. Chem. C* **2008**, *112*, 20227.
[61] S. J. Henley, R. A. Hatton, G. Y. Chen, C. Gao, H. Zeng, H. W. Kroto, S. R. P. Silva, *Small* **2007**, *3*, 1927.
[62] V. Saini, O. Abdulrazzaq, S. Bourdo, E. Dervishi, A. Petre, V. G. Bairi, T. Mustafa, L. Schnackenberg, T. Viswanathan, A. S. Biris, *J. Appl. Phys.* **2012**, *112*, 054327.
[63] P. H. Tan, A. G. Rozhin, T. Hasan, P. Hu, V. Scardaci, W. I. Milne, A. C. Ferrari, *Phys. Rev. Lett.* **2007**, *99*, 137402.
[64] P. H. Tan, T. Hasan, F. Bonaccorso, V. Scardaci, A. G. Rozhin, W. I. Milne, A. C. Ferrari, *Phys. E Low-dimensional Syst. Nanostruct.* **2008**, *40*, 2352.
[65] A. M. Crotty, A. N. Gizzi, H. J. Rivera-Jacquez, A. E. Masunov, Z. Hu, J. A. Geldmeier, A. J. Gesquiere, *J. Phys. Chem. C* **2014**, *118*, 19975.
[66] I. F. Perepichka, D. F. Perepichka, *Handbook of Thiophene-Based Materials: Applications in Organic Electronics and Photonics*, John Wiley & Sons, Chichester, UK **2009**.
[67] S. Casaluci, L. Cinà, A. Pockett, P. S. Kubiak, R. G. Niemann, A. Reale, A. Di Carlo, P. J. Cameron, *J. Power Sources* **2015**, *297*, 504.
[68] S. Ameen, M. A. Rub, S. A. Kosa, K. A. Alamry, M. S. Akhtar, H.-S. Shin, H.-K. Seo, A. M. Asiri, M. K. Nazeeruddin, *ChemSusChem* **2016**, *9*, 10.
[69] M. O. Reese, S. A. Gevorgyan, M. Jørgensen, E. Bundgaard, K. S. R. D. S. Ginley, D. C. Olson, M. T. Lloyd, P. Morvillo,

K. E. A. A. Elschner, O. Haillant, T. R. Currier, V. Shrotriya, M. Hermenau, M. Riede, K. R. Kirov, G. Trimmel, T. Rath, O. Inganas, F. Zhang, M. Andersson, K. Tvingstedt, M. Lira-Cantu, D. Laird, C. McGuiness, S. J. Gowrisanker, M. Pannone, M. Xiao, J. Hauch, R. Steim, D. M. DeLongchamp, R. Rosch, H. Hoppe, N. Espinosa, A. Urbina, G. Yaman-Uzunoglu, J.-B. Bonekamp, A. J. J. M. vanBreemen, C. Girotto, E. Voroshazi, F. C. Krebs, *Sol. Energy Mater. Sol. Cells* **2011**, *95*, 1253.

[70] C. Goh, R. J. Kline, M. D. McGehee, E. N. Kadnikova, J. M. J. Fréchet, *Appl. Phys. Lett.* **2005**, *86*, 122110.

[71] M. P. Arciniegas, F. Di Stasio, H. Li, D. Altamura, L. De Trizio, M. Prato, A. Scarpellini, I. Moreels, R. Krahne, L. Manna, *Adv. Funct. Mater.* **2016**, *26*, 4535.

[72] P. Wick, A. E. Louw-Gaume, M. Kucki, H. F. Krug, K. Kostarelos, B. Fadeel, K. A. Dawson, A. Salvati, E. Vázquez, L. Ballerini, M. Tretiach, F. Benfenati, E. Flahaut, L. Gauthier, M. Prato, A. Bianco, *Angew. Chem. Int. Ed.* **2014**, *53*, 7714.

[73] H. Ishii, K. Sugiyama, E. Ito, K. Seki, *Adv. Mater.* **1999**, *11*, 605.

[74] T. C. Sum, S. Chen, G. Xing, X. Liu, B. Wu, *Nanotechnology* **2015**, *26*, 342001.

[75] P. Schulz, E. Edri, S. Kirmayer, G. Hodes, D. Cahen, A. Kahn, *Energy Environ. Sci.* **2014**, *7*, 1377.

[76] A. Calloni, A. Abate, G. Bussetti, G. Berti, R. Yivlialin, F. Ciccacci, L. Duò, *J. Phys. Chem. C* **2015**, *119*, 21329.

[77] I. Chung, B. Lee, J. He, R. P. H. Chang, M. G. Kanatzidis, *Nature* **2012**, *485*, 486.

[78] M. Baghgar, M. D. Barnes, *ACS Nano* **2015**, *9*, 7105.

[79] E. V Canesi, M. Binda, A. Abate, S. Guarnera, L. Moretti, V. D'Innocenzo, R. S. S. Kumar, C. Bertarelli, A. Abrusci, H. Snaith, A. Calloni, A. Brambilla, F. Ciccacci, S. Aghion, F. Moia, R. Ferragut, C. Melis, G. Malloci, A. Mattoni, G. Lanzani, A. Petrozza, *Energy Environ. Sci.* **2012**, *5*, 9068.

[80] Z. Zhou, S. Pang, Z. Liu, H. Xu, G. Cui, *J. Mater. Chem. A* **2015**, *3*, 19205.

[81] F. Matteocci, G. Mincuzzi, F. Giordano, A. Capasso, E. Artuso, C. Barolo, G. Viscardi, T. M. Brown, A. Reale, A. Di Carlo, *Org. Electron.* **2013**, *14*, 1882.

[82] M. G. Helander, M. T. Greiner, Z. B. Wang, Z. H. Lu, *Appl. Surf. Sci.* **2010**, *256*, 2602.

[83] J. E. Mates, I. S. Bayer, M. Salerno, P. J. Carroll, Z. Jiang, L. Liu, C. M. Megaridis, *Carbon N. Y.* **2015**, *87*, 163.